



## Full Text View

[Volume 30, Issue 11 \(November 2000\)](#)

### Journal of Physical Oceanography

Article: pp. 2710–2722 | [Abstract](#) | [PDF \(745K\)](#)

# Marginal Thermobaric Stability in the Ice-Covered Upper Ocean over Maud Rise

**Miles G. McPhee**

*McPhee Research Company, Naches, Washington*

(Manuscript received July 30, 1999, in final form December 20, 1999)

DOI: 10.1175/1520-0485(2000)030<2710:MTSITI>2.0.CO;2

### ABSTRACT

Temperature ( $T$ ) and salinity ( $S$ ) profiles from the central Weddell Sea near the Maud Rise seamount measured during the 1994 Antarctic Zone Flux Experiment (ANZFLUX) have been analyzed for stability with respect to the thermobaricity, that is, the pressure dependence of thermal expansion rate. For many  $T$ – $S$  profiles in the region  $\Delta\rho$ , the difference between actual density (including the pressure contribution) and density of a water column with uniform temperature and salinity equal to that of the mixed layer, exhibits a maximum in the upper ocean within tens of meters of the mixed layer–pycnocline interface. Following work by K. Akitomo, if the mixed layer were to deepen and increase in density so that the  $\Delta\rho$  maximum coincided with the base of the mixed layer, the system would be thermobarically unstable and would overturn catastrophically. Thermobaric convection differs from convection driven by surface buoyancy flux (cooling and/or freezing) because once started, the production of turbulent mixing energy is derived from the water column instead of the surface, an important distinction in ice-covered oceans. A stability criterion is developed that considers the total sensible heat and latent heat of freezing required to drive a given  $T$ – $S$  profile to thermobaric instability, and is mapped in the Maud Rise region. A simple upper-ocean model, combined with enthalpy conservation at the ice–water interface and driven by surface stress and ice heat conduction observed with a drifting buoy cluster left in place after the ANZFLUX manned drift stations, is used to assess the susceptibility of observed profiles to thermobaric instability as the winter advanced. In the model, roughly one quarter of the profiles become unstable by the end of August, and it is argued that this may account for extensive polynya-like features that appeared in satellite microwave imagery over Maud Rise in August 1994, shortly after completion of the ANZFLUX Maud Rise drift.

#### Table of Contents:

- [Background](#)
- [Thermobaric stability](#)
- [The plausibility of Type](#)
- [Discussion](#)
- [REFERENCES](#)
- [FIGURES](#)

#### Options:

- [Create Reference](#)
- [Email this Article](#)
- [Add to MyArchive](#)
- [Search AMS Glossary](#)

#### Search CrossRef for:

- [Articles Citing This Article](#)

#### Search Google Scholar for:

- [Miles G. McPhee](#)

Thermal expansion of seawater depends on pressure, introducing a nonlinearity in the equation of state (thermobaricity) that may significantly enhance vertical mixing (Garwood et al. 1994; Løyning and Weber 1997). Akitomo (1999a) presents scaling formulas and stability criteria for deep open convection, and emphasizes the fundamental difference between homogeneous, “mixed layer” convection (Type I) and thermobarically driven, “two-layer” convection (Type II), where the latter derives mainly from the pressure dependence of the thermal expansion factor for seawater. Type I convection requires a continuous source of destabilizing surface buoyancy flux, while Type II supplies its own buoyancy flux in downwelling plumes, often of much larger magnitude locally (Akitomo et al. 1995) than the surface buoyancy flux needed to initially trigger convection in either sense. A requirement for Type II convection is that cold, relatively fresh water overlies warm, more saline water, typical of most high-latitude oceans.

Although thermobaricity is potentially important for high-latitude deep convection anywhere (Garwood 1991), Akitomo shows that for Type II convection, the destabilizing tendency of thermobaricity must overcome the background stratification associated with the salinity gradient. He identifies a simple criterion for thermobaric instability using bulk properties of the water column as defined in Fig. 1. The strength of the thermobaric tendency must exceed the background stratification for Type II convection:

$$\alpha_1 \Delta \theta_1 > (\alpha_0 \Delta \theta_2 + \beta \Delta S_2) / H_2,$$

where  $\alpha_1$  is the slope of the linearized thermal expansion factor:  $\alpha(z) = \alpha_0 + \alpha_1 z$  and  $\beta$  is the saline contraction factor. The inequality may be expressed as

$$\frac{H_2}{H_\alpha} \theta_{\text{plume}} > S_{\text{deep}} + 1,$$

where

$$\theta_{\text{plume}} = \Delta \theta_1 / \Delta \theta_2 \quad (1)$$

is Akitomo’s *normalized strength of thermobaricity*,  $S_{\text{deep}} = \beta \Delta S_2 / \alpha_0 \Delta \theta_2$  is normalized background haline stratification, and  $H_\alpha = \alpha_0 / \alpha_1$  is the characteristic thermobaric depth. Akitomo shows that for temperature and salinity structure in the central and eastern Weddell Sea,  $\theta_{\text{plume}}$  generally falls above (i.e., on the unstable side of) a line defined by

$$\theta_{\text{plume}} = (H_\alpha / H_2) (1 + S_{\text{deep}}) \quad (2)$$

representing marginal stability. In contrast,  $\theta_{\text{plume}}$  calculated from profiles in the Greenland Sea cluster below the line, indicating stability in the thermobaric sense (see Fig. 10 of Akitomo 1999a).

In the late 1970s, satellite passive microwave imagery revealed a large expanse of open water (or low concentration sea ice) that persisted for several seasons well within the confines of the annual sea ice limits of the Weddell Sea. This coherent feature (the Weddell polynya) apparently first formed over the Maud Rise region (a bathymetric highland centered near 65°S, 3°E), then migrated slowly westward, leaving evidence of deep convection (Gordon 1978) and significant impact on deep-water production and properties (Gordon 1991). Despite its disappearance two decades ago, interest in the Weddell polynya has remained high because it may have represented a completely different mode of air–sea–ice interaction (Gordon 1991), one in which sea ice formation is relatively rare and ephemeral, and there is much more direct exchange between the atmosphere and deep ocean. Widespread reappearance of these conditions could conceivably impact global climate. Large areas of open water/thin ice have, in fact, been observed well within the seasonal ice limits in the Weddell and Cosmonaut Seas on several occasions since the Weddell polynya (e.g., Comiso and Gordon 1996), but so far none has exhibited anywhere near the area and persistence of the feature seen in the 1970s.

Winter observations (e.g., Martinson and Iannuzzi 1998) have shown that static stability of the eastern Weddell is so weak in many locations that a few tenths of a meter of additional ice growth would densify the mixed layer enough to trigger surface-buoyancy-driven free convection [Akitomo’s (1999a) Type I]. It is germane to ask why deep convection is not observed more often. The answer lies with the flux of heat into the mixed layer from below. Relatively warm water in the pycnocline presents a *thermal barrier* (Martinson 1990) that severely curtails ice growth during winter: as the mixed layer deepens in response to salt rejection from growing sea ice, heat entrained from below exerts a powerful negative feedback. Martinson and Iannuzzi (1998) analyzed available measurements from the Weddell in terms of units of buoyancy, which they express as equivalent ice growth. They define the bulk stability by the equivalent ice growth needed to mix the upper ocean



to the level in the permanent pycnocline where subsequent convection may be maintained by surface cooling alone.<sup>1</sup> All of the profiles in their study exhibit bulk stability (they all have surface mixed layers), but in some regions (notably over Maud Rise) the total equivalent growth required for deep convection is much less than 1 m, in agreement with [Akitomo's \(1999a\)](#) assessment. [Martinson and Iannuzzi \(1998\)](#) did not consider the influence of thermobaricity in their analysis.

Documenting the processes that control ocean heat flux during winter provided the primary rationale for the Antarctic Zone Flux Experiment (ANZFLUX) in 1994 ([McPhee et al. 1996](#)). Both direct flux measurements from manned drift stations and parameterized heat flux inferred from drifting buoy measurements confirmed that ocean heat flux is large in the central Weddell, averaging  $52 \text{ W m}^{-2}$  during one of the 5-day manned drifts and  $27 \text{ W m}^{-2}$  for the season-long buoy drift ([McPhee et al. 1999](#)). It was also highly episodic, depending on the surface friction velocity and elevation of mixed layer temperature above freezing. Large ocean heat flux during storms caused significant basal melting of the thin ice cover, but growth between storms was enough to maintain a mean thickness that approximately balanced conductive heat flux in the ice with ocean heat flux from below through August and much of September ([McPhee et al. 1999](#)). Regional values of heat flux inferred from mixed-layer tracer distributions agreed reasonably well with local measurements (Muench et al. 1999, manuscript submitted to *J. Geophys. Res.*).

An intriguing epilogue of the 1994 ANZFLUX project was that subsequent analysis of active and passive microwave imagery showed a fairly widespread region of open water and/or low concentration ice that appeared over Maud Rise shortly after our departure at the end of the second (Maud Rise) manned drift ([Drinkwater 1996](#); personal communication 1995). It persisted for several weeks. A number of energetic storms were encountered during the manned phase of the project (including one with hurricane force winds shortly after the Maud Rise drift), and are also evident in the buoy record following our departure. This paper examines whether conditions observed during the Maud Rise drift of ANZFLUX 94, and in the subsequent buoy data, were conducive to the onset of Type II thermobaric instability within a short time after our departure on 9 August 1994. The approach is as follows. In [section 2](#), a stability criterion is developed that takes into account the thermal barrier ([Martinson 1990](#)). It identifies for a given temperature and salinity profile the buoyancy removal required to drive the system to thermobaric instability, and is applied to temperature ( $T$ ) and salinity ( $S$ ) profiles measured during the Maud Rise drift. In [section 3](#), a horizontally homogeneous, numerical boundary layer model adapted from [McPhee et al. \(1999\)](#) is combined with a simple thermodynamic ice model to estimate heat and buoyancy flux at the ice–ocean interface. The model is initialized with observed  $T$ – $S$  profiles, then forced by surface stress and ice heat conduction estimated from data gathered by a remote buoy cluster deployed west of Maud Rise ([McPhee et al. 1999](#)). The object is to test the plausibility of Type II convection occurring under realistic forcing. Results and outstanding research issues are discussed in [section 4](#).


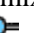
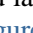
## 2. Thermobaric stability during ANZFLUX

Accurate conductivity–temperature–depth (CTD) profiles were measured during ANZFLUX with two different Sea-Bird Electronics SBE 9+ systems. CTD/tracer stations were taken using the ship SBE 9+ CTD/rosette sampling system during transits into (including a survey pattern around the site of the first, “warm regime” drift) and out of the ice, between the drift camps, and daily while the drift camps were occupied. A separate system was set up on the ice during the drift camps to sample more frequently in “yo-yo” mode; a total of 148 yo-yo casts were made ([Huber et al. 1995](#)).

For a regional overview,  $\theta_{\text{plume}}$  was calculated for the ship CTD casts according to (1) using definitions provided by [Fig. 1](#)  following [Akitomo \(1999a\)](#). All of the casts fell above the marginal stability line (2), with some casts reaching values exceeding 8 for the normalized thermobaricity strength. The geographic distribution of  $\theta_{\text{plume}}$  ([Fig. 2](#) ) shows that the maximum departures from marginal stability occur in the water column over Maud Rise.

Following Akitomo's approach, quantitative estimates of the amount of buoyancy that must be removed from the system to trigger Type II overturn may be made as follows.

### a. An idealized, two-layer system

Consider first an idealized two-layer system based on ship CTD number 50, which is the station with the largest thermobaricity strength in the series of casts made with the ship's CTD system ([Fig. 2](#) ). The idealized profile consists of a mixed layer with observed properties overlying a lower layer with mean properties equal to averages in the water column from the mixed layer base to the temperature maximum. Potential density of the system is indicated by the dashed lines in [Fig. 1c](#) . [Figure 3](#)  illustrates that the idealized situation is relatively close to Type I convective entrainment. Increasing salinity by 0.05 psu, corresponding to ice growth of about 30 cm, would increase mixed layer density enough to match the lower layer. However, buoyant convection would cease as soon as warm water mixed from the lower layer supplied enough surface heat flux to stop ice growth. In the Weddell Sea there is almost always a significant thermal barrier preventing sustained ice growth ([Martinson and Iannuzzi 1998](#)). So although pure convective mixing could occur with relatively little additional ice growth, it is difficult to visualize how Type I convection remains active long enough to reach deep levels.

Consider next thermobaricity. Here pressure is included in the in situ density  $[\rho(\theta, S, p)]$  using the UNESCO equation of state (Gill 1982). For the two-layer ocean of Fig. 3, the difference between actual density and density of an ocean with uniform temperature and salinity equal to the mixed layer values:  $\Delta\rho = \rho(\theta, S, p) - \rho(\theta_{\text{ml}}, S_{\text{ml}}, p)$  is shown as the solid curve in Fig. 4. It is like Akitomo's schematic (1999a, his Fig. 7) except that  $\Delta\rho$  is defined with opposite sign, and he uses a linearized version of the equation of state with constant vertical gradient for the thermal expansion coefficient. Note that  $\Delta\rho$  is everywhere positive below the mixed layer (in the domain shown), but decreases with increasing depth. Thermobaric instability is illustrated by the dashed line. If mixed layer salinity is increased by just enough to eliminate the density difference between water types with mixed layer and lower-layer  $T$ - $S$  characteristics, at pressure corresponding to the depth of the mixed layer,  $\Delta\rho$  is zero or negative for all depths. In this case, a parcel of water displaced downward from the original mixed layer interface will continue to sink, being denser than surrounding fluid. For instability, the idealized system would require an increase of 0.04 psu in mixed layer salinity, supplied by about 23 cm of ice growth.

As Akitomo points out, once triggered, the process no longer depends on destabilizing surface buoyancy flux. Using his scaling, an estimate of buoyancy flux in Type II convection for Weddell-like conditions is

$$\langle w'b' \rangle_{\text{plume}} \sim \alpha_1 \Delta\theta g l_{\text{on}}^2 f \sim 1 \times 10^{-5} \text{ W kg}^{-1}, \quad (3)$$

where  $\Delta\theta$  is the difference in temperature across the pycnocline,  $g$  is the acceleration of gravity,  $l_{\text{on}}$  is the horizontal plume length scale, and  $f$  is the Coriolis parameter. For comparison, an upper limit for heat flux reaching the ice in extreme melting conditions ( $u_* \sim 0.03 \text{ m s}^{-1}$ ,  $\delta T \sim 2\text{K}$ ) would be  $\sim 1000 \text{ W m}^{-2}$  (McPhee et al. 1999), corresponding to a melt rate  $\sim 0.5 \text{ m d}^{-1}$  and stabilizing surface buoyancy flux  $\langle w'b' \rangle_0 \sim 1 \times 10^{-6} \text{ W kg}^{-1}$ . This would eliminate a typical eastern Weddell Sea ice cover in about a day, yet is still an order of magnitude less than the destabilizing buoyancy encountered in thermobarically unstable plumes, according to (3). Thus even in the most extreme melting conditions, the idealized system would remain convective unless the area occupied by downwelling plumes was less than about 10% of the total area.

### b. Continuous temperature and salinity profiles

In reality, the upper ocean is not two layered, and continuous stratification in the pycnocline tends to increase its resistance to thermobaric overturn. The thermobaric density barrier,  $\Delta\rho = \rho(T, S, p) - \rho(T_{\text{ml}}, S_{\text{ml}}, p)$  for the actual  $T$ - $S$  profiles for ship station 50 is shown in Fig. 5a. The maximum in  $\Delta\rho$  occurs at about 160 dbar, below which its slope is negative. By analogy with the two-layer system, the integral of  $\Delta\rho_{\text{max}} - \Delta\rho$  over the water column above that level provides an estimate of the additional mass needed to destabilize the system, as indicated by the shaded area: about  $3.6 \text{ kg m}^{-2}$ . Unlike the idealized case, the layer separating the mixed layer and the  $\Delta\rho_{\text{max}}$  level carries considerable heat (relative to the mixed layer) as indicated by the shaded area in Fig. 5b. In order for the system to reach thermobaric instability, heat from this layer must be entrained into the mixed layer and vented. For this case, the heat above  $\Delta\rho_{\text{max}}$  amounts to about  $127 \text{ MJ m}^{-2}$ . As this water cools, it loses buoyancy:  $\text{Mass}_{\text{ocean}} = -1.5 \text{ kg m}^{-2}$ , a fair proportion of the mass deficit. The remaining density increase would require a modest amount of ice growth, about 10 cm, with a latent heat loss of about  $24 \text{ MJ m}^{-2}$  bringing the total required heat loss to  $151 \text{ MJ m}^{-2}$ . Thus to overturn this system within a month would require a sustained net outward heat flux of about  $57 \text{ W m}^{-2}$ , along with enough turbulent mixing to increase the mixed layer depth to around 160 m. This is not impossible, but also not too likely. During ANZFLUX measurements over Maud Rise, the average ocean heat flux was about half this value (McPhee et al. 1999).

It appears that when detailed profiles are available, a useful measure of thermobaric stability is the *thermobaric barrier*,  $H_{\text{tot}}$ , equal to the total heat loss (including latent heat of freezing) required to densify the water column enough to eliminate  $\Delta\rho_{\text{max}}$ . Obviously, the most likely candidates for overturn are profiles where this level is near the mixed layer depth. ANZFLUX profiles from west of Maud Rise (in the "warm regime" where the maximum temperature in the water column was higher) typically had relatively deep  $\Delta\rho_{\text{max}}$  levels, with much larger heat content in the intermediate layer ( $\sim 2000 \text{ MJ m}^{-2}$ ). To vent heat upward from these intermediate layers would require both unrealistic surface heat loss and an inordinate amount of turbulent mixing, hence the profiles may be considered thermobarically stable, even though they lie above the marginal stability line (2). Ship CTD profiles for which  $H_{\text{tot}} < 100 \text{ MJ m}^{-2}$  are marked with pentagrams in Fig. 2. These are likely candidates for Type II convection, since the required heat loss over the next month is comparable to the average heat flux out of the water column inferred from buoy measurements (McPhee et al. 1999). Note that they do not necessarily coincide with the maximum values of  $\theta_{\text{plume}}$ , because the bulk criterion does not explicitly account for the potentially

important thermal barrier between the mixed layer and  $\Delta\rho_{\max}$ .

A more detailed CTD record exists from the series of yo-yo casts made at frequent intervals during the Maud Rise manned drift station, 2–8 August 1994. One of the least thermobarically stable CTD stations was yo-yo cast YU075 (Fig. 6). Corresponding  $\Delta\rho$  and heat content profiles (Fig. 7) show that relatively little sensible heat loss ( $22 \text{ MJ m}^{-2}$ ) and ice growth (latent heat loss equal to  $25 \text{ MJ m}^{-2}$ ) would instigate Type II convection. Total heat loss requirements for all of the yo-yo profiles taken during the Maud Rise drift were calculated and are mapped along with bathymetry in Fig. 8. The least stable profiles are found between the 2500-m and 3000-m isobaths, on the east slope of the rise. Similar results were obtained from the ship CTD record (low stability profiles marked by pentagrams in Fig. 2), including station 47 during our approach up the west slope. The steplike structures immediately below the mixed layer (Fig. 6) appear to play an important role in Type II stability, and are discussed in section 4.

Although the normalized strength of thermobaricity over Maud Rise was generally large, many of the yo-yo profiles were reasonably stable with regard to  $H_{\text{tot}}$ . Consider the first deep yo-yo cast (YU043) during the Maud Rise drift. Its value for  $\theta_{\text{plume}}$  was high (7.4), but so was its thermobaric barrier:  $H_{\text{tot}} = 369 \text{ MJ m}^{-2}$  (Fig. 9). Compared with cast YU075, this profile would require several times the heat extraction for instability. If a mechanism for mixing and cooling the water above 175 m (the  $\Delta\rho_{\max}$  level) could be identified, it would provide enough density increase for instability without additional ice growth. An intense storm (common in the Weddell) could furnish the initial mixing to begin venting the thermocline, however, the upward heat flux in the mixed layer would soon cause melting, which would stabilize the boundary layer. Without invoking strong horizontal inhomogeneity (e.g., rapid ice divergence), it thus seems unlikely that surface-driven processes could destabilize a widespread area with upper-ocean structure like YU043.

### 3. The plausibility of Type II convection in 1994

Figures 5, 7, and 9 show that details of density structure in the upper part of the pycnocline determine to large degree which profiles from among many with similar bulk characteristics are susceptible to Type II convection. The process depends critically on venting sensible heat from the thermal barrier above  $\Delta\rho_{\max}$  into the mixed layer and then to the surface, without simultaneously melting enough ice to form a new, shallower mixed layer. No direct measurements of upper ocean  $T$ - $S$  structure or surface flux conditions were made in the immediate vicinity of the Maud Rise drift subsequent to our departure from the area, so by necessity, any assessment as to whether Type II convection could account for widespread sea ice opening over Maud Rise in mid-to-late August involves conjecture. The approach taken here is to combine a simple prognostic *local turbulence closure* (LTC) upper-ocean model (McPhee 1999) with the heat and mass balance at the ice-ocean interface driven by surface fluxes derived from a buoy cluster left at the site of the first (“Warm Regime”) ANZFLUX drift (McPhee et al. 1999).

The boundary-layer turbulence model works as follows. For each time step, the mixing length is calculated based on surface stress, surface buoyancy flux, displacement from the ice-ocean interface, and pycnocline depth, following the algorithm described by MCPhee (1994). The pycnocline depth is defined as the depth where the squared buoyancy frequency first exceeds a threshold value:

$$N^2 = -\frac{g}{\rho} \frac{\partial\rho}{\partial z} \geq 1.5 \times 10^{-5} \text{ s}^{-2}.$$

Using an estimate of eddy viscosity based on the surface friction velocity and mixing length, an initial guess for the distribution of friction velocity in the boundary layer is made by solving the analytic Ekman stress equation, and eddy viscosity and scalar diffusivity are computed from the product of friction velocity and mixing length. If significant momentum and buoyancy fluxes exist at the pycnocline depth, they are used to calculate mixing length and eddy diffusivities in the pycnocline. The refined estimate of eddy viscosity is then used to solve for stress ( $u_*$ ) numerically. The process is iterated until a convergence criterion is satisfied. Originally developed for extending flux measurements through the boundary layer (McPhee et al. 1999), the model calculates eddy viscosity/diffusivity based only on the current surface fluxes and  $T$  and  $S$  profiles, either observed or taken from the previous time step in a numerical simulation. It does not carry *prognostic equations* for momentum or turbulence quantities. For numerical simulation, conservation equations for temperature and salinity are stepped forward by a leapfrog method in time, using an implicit solution in the vertical (McPhee 1999). Surface buoyancy flux, which plays an important role in setting the turbulence scales, depends mainly on salinity flux, proportional to the ice growth rate. Enthalpy is conserved at the ice-ocean interface so that any imbalance in conductive versus ocean heat results in ice growth or ablation.

The model was initialized with the YU075 temperature and salinity profiles and run for 25 days starting from the time of the observation (year day 216.78). Surface flux conditions were estimated from data obtained with a buoy cluster deployed

at the end of the Warm Regime station in late July. During mid-August the buoy drifted over the abyssal plain about 250 km southwest of Maud Rise. In the earlier paper, interfacial stress and conductive heat flux through the ice cover were calculated from the buoy data (McPhee et al. 1999, their Figs. 9 and 11). Here the same values are taken as representative of conditions over Maud Rise, except that ice conductive heat flux was multiplied by the ratio of mean ice thickness at the buoy location (60 cm) to the ice thickness calculated in the model, starting from the observed thickness of 35 cm at the Maud Station site. Assuming that the upper-surface thermal driving is about the same, the thermal gradient in the ice should vary approximately inversely as the ice thickness ratio, consistent with the idea that the relatively thin ice encountered over Maud Rise would grow toward a mean thickness that balanced conductive and ocean heat flux. The model takes no explicit account of thermobaric instability; however, at each time step the total heat loss ( $H_{\text{tot}}$ ) and mass deficit required to drive the  $\Delta\rho$  profile to instability were calculated. The presumption is that, if these quantities go to zero, the water column would undergo Type II convection.

Model results are summarized in Fig. 10. Prescribed surface friction velocity and ice conductive heat flux based on the buoy results are shown in Fig. 10a. Computed ocean-to-ice heat flux and ice thickness determined by enthalpy conservation (Fig. 10b) show that for the first fortnight, conduction exceeds ocean heat flux so that the ice grows, albeit slowly. This is critical since the destabilizing buoyancy flux associated with salt rejection, combined with several energetic drift events, keeps the mixed layer deep (Fig. 10c). The main result is shown in Fig. 10d. By late on day 227, the water column above  $\Delta\rho_{\text{max}}$  has vented enough heat and gained enough salinity from freezing to force Type II convection.

Although Type II convection would completely change the upper-ocean turbulence regime after day 228, the LTC model time series in Fig. 10 are extended for the entire 25-day run because they illustrate interesting characteristics of the system that might be expected in the absence of thermobaricity. Note the event in the (nonthermobaric) simulation starting at about day 231. Ocean heat flux (solid curve in Fig. 10b) increases dramatically, reflecting a rapid rise in upper-ocean temperature. The dynamic mixed layer (i.e., based on the density gradient) essentially fills the vertical domain (Fig. 10c), thus for turbulence the entire upper ocean appears to be near neutral stratification. However, the halocline, defined by the depth at which salinity exceeds its near-surface value by 0.02 psu (labeled “Scalar Mixed Layer Depth” in Fig. 10c) remains near its previous level for several days, then begins to shoal. What happens in the model is that by day 231 the mixed layer has lost enough buoyancy to instigate Type I convection into the stielike layer below. The potential density of this layer is very close to the mixed layer density, and initially there is rapid mixing that warms the mixed layer and increases ocean heat flux to the ice (Fig. 11a). Surface buoyancy flux from melting then reduces the turbulence scales and constrains turbulent mixing to the upper part of the water column, hence the freshening and cooling near the surface apparent in Fig. 11a after the abrupt convection event. So, although density stratification remains low, the thermal barrier effect dominates Type I convection by limiting turbulence scales. If ice were not present, direct cooling would drive deep convection, sustained by upwelling warm water and no longer inhibited by stabilizing surface buoyancy flux.

As a thought experiment consider the one-dimensional LTC model modified so that after the transition to thermobaric instability at about day 227.75, its turbulence scales no longer depend on surface conditions but instead are driven by the conversion of potential energy of the entire thermobaric water column to turbulent kinetic energy. By scaling arguments, a parameterization for eddy diffusivity in this case would be

$$K_H = \frac{A^3 w_{\text{plume}}^4}{\langle w'b' \rangle_{\text{plume}}}, \quad (4)$$

where  $w_{\text{plume}}$  and  $\langle w'b' \rangle_{\text{plume}}$  are representative thermobaric plume velocity and buoyancy flux, respectively, and  $A$  is a factor incorporating in some way the fractional area occupied by the plumes. From Akitomo’s (1999b) numerical modeling results, it appears that a reasonable range for  $K_H$  might be from 0.1 to 1  $\text{m}^2 \text{s}^{-1}$ . For concreteness, a value of 0.2  $\text{m}^2 \text{s}^{-1}$  was chosen, coinciding with the *maximum* value reached in the combined shear and buoyancy-driven mixed layer before the onset of thermobaricity. This value was assigned to the whole model domain after day 227.75. The ensuing salinity and thermal structure (Fig. 11b) shows that mixing is rapid and relatively complete. Heat flux from below, forced in the model by maintaining the temperature of the lowest grid point at its initial value, averages about 1.3  $\text{kW m}^{-2}$  after day 228. The ice melts rapidly with the warming water temperature, going from 0.45 m thick to open water in about 3 days.

Out of 102 yo-yo CTD stations during the Maud Rise drift, 38 had thermobaric barrier values of 100  $\text{MJ m}^{-2}$  or less (based on the upward profiles, which usually had sharper definition of the steps). Each of these stations was used to initialize the temperature, salinity, and start time for one-dimensional model runs. Of the 38 model runs, 27 (indicated by pentagrams in Fig. 8) reached thermobaric instability conditions (i.e., the mass deficit and thermobaric barrier both reached zero) before the end of August. The modeling approach has obvious shortcomings: (a) the calculations were driven by surface conditions measured 250 km away; (b) modeled values of  $H_{\text{tot}}$  are sensitive to slight changes in the initial profiles (e.g., there were several instances where initializing with the up- or downtrace of a particular station yielded conflicting

results); (c) divergence of the ice cover and Ekman transport in the mixed layer was neglected; and (d) particularly in the Maud Rise region, any assumption of horizontal homogeneity implicit in one-dimensional modeling is suspect. Nevertheless, the exercise illustrates that perhaps a quarter or more of the upper-ocean conditions we observed over Maud Rise were susceptible to Type II thermobaric convection before the end of winter.

#### 4. Discussion

A simple one-dimensional model, initialized with several different temperature/salinity profiles observed over Maud Rise in early August, then forced by plausible time series of surface friction velocity and ice heat conduction obtained from drifting buoy observations, was found to reach a thermobarically unstable state by mid- to late August (times ranging from day 227 to 242). When thermobaric enhancement of turbulence (as discussed, e.g., by [Garwood 1991](#)) was neglected, densification of the surface mixed layer in some instances led to Type I convection and a short period of intense mixing and increased ocean heat flux, but there was no sustained deep convection or elimination of the ice cover. When a crude treatment of enhanced mixing due to thermobaricity was included by simply assigning a high (though plausible) value for eddy diffusivity, the model produced open water within a few days. The results thus support [Akitomo's \(1999a\)](#) assertion that thermobaricity is a critical factor in deep convection in the Weddell Sea. Intense ocean heat flux from such convection is a likely cause of persistent low ice concentrations reported by [Drinkwater \(1996\)](#) in satellite microwave imagery over Maud Rise in late winter 1994.

The marginally stable profiles identified in [Fig. 8](#) all have in common that the  $T$ - $S$  structure is steplike just below the existing mixed layer (e.g., [Fig. 6](#)). In the model, the extremely sharp interface between the mixed layer and next lower step reduces the thermal barrier enough to reach conditions allowing Type II convection. L. Padman (1999, personal communication) discusses sub-mixed-layer steps observed during ANZFLUX in the context of *cabbeling*, a potential source of interior mixing deriving from the temperature dependence (rather than pressure dependence) of the thermal expansion coefficient. Because of curvature of isopycnals in  $T$ - $S$  space, diapycnal mixing may result if two water types with slightly different density (i.e., statically stable) but differing  $T$ - $S$  properties are combined, since the resulting mixture may be denser than either parent type. Padman shows evidence that the ice station drifted through an active cabbeling event on day 218 (centered near the time of yo-yo cast 110 in [Fig. 8](#)). In his interpretation, mixed layer water of slightly enriched salinity was advected during a storm over a filament of Warm Deep Water (WDW) uplifted along the flanks of Maud Rise. Mixing near the base of the narrow pycnocline separating the surface layer from the deeper, subsurface WDW layer created a cabbeling-effect density anomaly, leading to energetic overturn in the subsurface layer. The latter thickened and cooled rapidly by mixing pycnocline water from above, that is, at the expense of the surface layer, which warmed slightly. The result is a sharpening of the interface between the layers, but unlike most convective scenarios, the pycnocline shoals because the subsurface layer grows *upward*. Like Type I convection, the cabbeling process in isolation is self-limiting when there is a sea ice cover because positive buoyancy from melting accompanies enhanced heat flux. However, it is obvious that both the pressure and temperature dependence of the thermal expansion factor are important in the equation of state and may work together to effect deep convection. At the least, cabbeling may provide an important preconditioning for thermobaric instability.

The presence of the steplike structures below the mixed layer is important for low values of  $H_{\text{tot}}$ , but their persistence in the face of highly energetic mixing from storms that regularly traverse this region is problematic. This is the main drawback to the approach taken in this paper. Variability in the upper boundary and vertical extent of the pycnocline in the Weddell Sea was a central feature of our ANZFLUX findings ([McPhee et al. 1996](#)), and of other oceanographic buoy data from the region (C. Kottmeier 1996, personal communication). This variability, coupled with Ekman shear from frequent storms with boundary shear stress approaching 1 Pa, would seem to limit the persistence of the steps and the utility of modeling that assumes horizontally homogeneous conditions. On the other hand, given the marginal static stability of the upper ocean, especially over Maud Rise ([Martinson and Iannuzzi 1998](#)), shear and associated differential advection in the system may be continually creating steps by several possible mechanisms, including cabbeling (L. Padman 1999, personal communication), double-diffusive convection ([Robertson et al. 1995](#)), limited regions of Type I or II convection ([Akitomo 1999a,b](#)), or enhanced turbulence in the pycnocline from differential advection of horizontal density gradients ([Crawford et al. 1999](#)). Our understanding of these processes, as well as basic knowledge of how turbulent mixing occurs near the interface between the mixed layer and pycnocline, is rudimentary at best, and the need for further theoretical, numerical modeling, and observational work is clear.

#### Acknowledgments

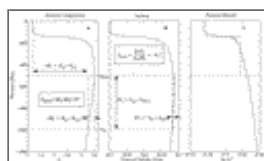
Comments on the original manuscript by L. Padman, R. Muench, and an anonymous reviewer are much appreciated. B. Huber kindly supplied the ANZFLUX CTD data. Research support from the National Science Foundation under Grants OPP-9319520 and OPP-9728837, and from the Office of Naval Research Contract N00014-96-C-0032 is gratefully acknowledged.

## REFERENCES

- Akitomo, K., 1999a: Open-ocean deep convection due to thermobaricity. 1. Scaling argument. *J. Geophys. Res.*, **104**(C3), 5225–5234.
- , 1999b: Open-ocean deep convection due to thermobaricity. 2. Numerical experiments, *J. Geophys. Res.*, **104**(C3), 5235–5249.
- , T. Awaji, and N. Imasato, 1995: Open-ocean deep convection in the Weddell Sea: Two-dimensional numerical experiments with a nonhydrostatic model. *Deep-Sea Res. I*, **42**, 53–73.
- Comiso, J. C., and A. L. Gordon, 1996: Cosmonaut polynya in the Southern Ocean: Structure and variability. *J. Geophys. Res.*, **101**(C8), 18 297–18 313.
- Crawford, G., L. Padman, and M. McPhee, 1999: Turbulent mixing in Barrow Strait. *Contin. Shelf Res.*, **19**, 205–245.
- Drinkwater, M. R., 1996: Satellite microwave radar observations of climate-related sea-ice anomalies. *Workshop on Polar Processes in Global Climate*, Cancun, Mexico, Amer. Meteor. Soc., 115–118.
- Garwood, R. W., Jr., 1991: Enhancements to deep turbulent entrainment. *Deep Convection and Deep Water Formation in the Oceans*, P. C. Chu and J. C. Gascard, Eds., Elsevier, 197–213.
- , S. M. Isakari, and P. C. Gallacher, 1994: Thermobaric convection. *The Polar Oceans and Their Role in Shaping the Global Environment, Geophys. Monogr.*, No. 85, Amer. Geophys. Union, 199–209.
- Gill, A. E., 1982. *Atmosphere–Ocean Dynamics*. Academic Press, 661 pp.
- Gordon, A. L., 1978: Deep Antarctic convection of Maud Rise. *J. Phys. Oceanogr.*, **8**, 600–612. [Find this article online](#)
- , 1991: Two stable modes of Southern Ocean winter stratification. *Deep Convection and Deep Water Formation in the Oceans*. Elsevier Oceanography Series, Vol. 57, Elsevier, 17–35.
- Huber, B., P. Schlosser, and D. G. Martinson, 1995: Thermohaline structure and tracer studies during ANZFLUX. *Antarctic J. U.S.*, **30**, 129–130.
- Løyning, T. B., and J. E. Weber, 1997: Thermobaric effect on buoyancy-driven convection in cold seawater. *J. Geophys. Res.*, **102**, 27 875–27 885.
- Martinson, D. G., 1990: Evolution of the Southern Ocean winter mixed layer and sea ice: Open ocean deepwater formation and ventilation. *J. Geophys. Res.*, **95**, 11 641–11 654.
- , and R. A. Iannuzzi, 1998: Antarctic ocean–ice interaction: Implications from ocean bulk property distributions in the Weddell Gyre. *Antarctic Sea Ice: Physical Processes, Interactions and Variability*, Antarctic Research Series, Vol. 74, Amer. Geophys. Union 243–271.
- McPhee, M. G., 1994: On the turbulent mixing length in the oceanic boundary layer. *J. Phys. Oceanogr.*, **24**, 2014–2031. [Find this article online](#)
- , 1999: Parameterization of mixing in the ocean boundary layer. *J. Mar. Syst.*, **21**, 55–65.
- , and Coauthors, 1996: The Antarctic Zone Flux Experiment. *Bull. Amer. Meteor. Soc.*, **77**, 1221–1232. [Find this article online](#)
- , C. Kottmeier, and J. Morison, 1999: Ocean heat flux in the central Weddell Sea during winter. *J. Phys. Oceanogr.*, **29**, 1166–1179. [Find this article online](#)
- Robertson, R. A., L. Padman, and M. D. Levine, 1995: Fine structure, microstructure, and vertical mixing processes in the upper ocean in the western Weddell Sea. *J. Geophys. Res.*, **100**, 18 517–18 535.

---

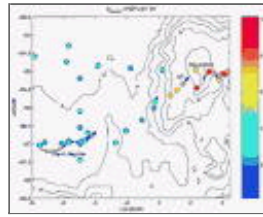
## Figures



[Click on thumbnail for full-sized image.](#)

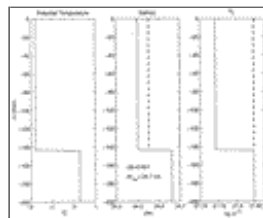


Fig. 1. Upper-ocean properties from Ship Station 50, 1994 ANZFLUX project in the Weddell Sea. (a) Potential temperature, showing definitions for [Akitomo's \(1999a\)](#) normalized strength of thermobaricity ( $h_{ref}$  is a reference level well below the temperature and salinity maxima, taken to be the 1000-db level to coincide with Akitomo's treatment). (b) Salinity, showing definitions for the normalized background haline stratification. (c) Potential density [ $\rho(T, S, p = 0) - 1000$ ] with dashed lines representing an idealized, two-layer system



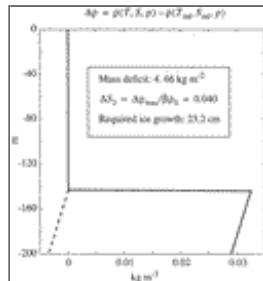
Click on thumbnail for full-sized image.

Fig. 2. Map of  $\theta_{plume}$  for ship CTD stations during ANZFLUX superimposed on bathymetric contours (km). Solid curves marked Warm Regime and Maud Rise indicate drift trajectories during the two manned drift camps. Color indicates the magnitude of  $\theta_{plume}$  according to the scale at right. Pentagrams indicate ship stations with  $H_{tot} < 100 \text{ MJ m}^{-2}$



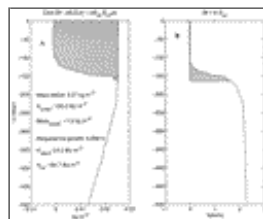
Click on thumbnail for full-sized image.

Fig. 3. Temperature, salinity, and  $\sigma_0$  for the idealized two-layer system of [Fig. 1c](#). The dashed lines indicate the increase in salinity and  $\sigma_0$  necessary for Type I convection



Click on thumbnail for full-sized image.

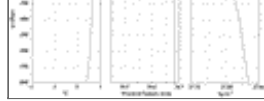
Fig. 4. The thermobaric density barrier for the idealized two-layer system of [Fig. 3](#), i.e., the difference between density (including contraction due to pressure) and density of an upper ocean with uniform temperature and salinity equal to mixed layer values. The dashed line indicates  $\Delta\rho$  if mixed layer salinity were increased by 0.04 psu, which is thermobarically unstable



Click on thumbnail for full-sized image.

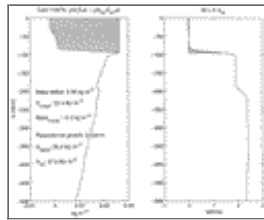
Fig. 5. Diagram showing definitions for the thermobaric barrier,  $H_{tot}$  (a) Profile of  $\Delta\rho$  for station 50. The shaded area represents the added mass needed to densify the water column above  $\Delta\rho_{max}$  to thermobaric instability. (b) Temperature relative to mixed layer temperature. The shaded area represents the sensible heat in the water column that must be vented to deepen the mixed layer to the  $\Delta\rho_{max}$  level





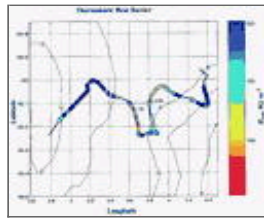
Click on thumbnail for full-sized image.

Fig. 6. Upper-ocean properties for ANZFLUX yo-yo station YU075 during the Maud Rise drift



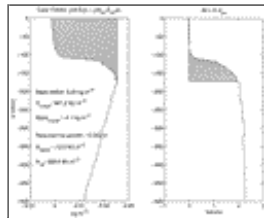
Click on thumbnail for full-sized image.

Fig. 7. Thermobaric barrier diagram for station YU075



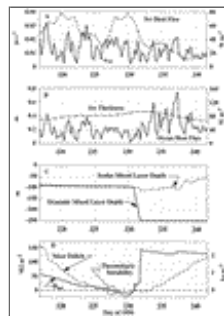
Click on thumbnail for full-sized image.

Fig. 8. Map showing thermobaric barrier values for the yo-yo stations during the ANZFLUX Maud Rise drift, superimposed on bathymetry (km). Redder colors are less stable. Pentagrams mark stations for which the one-dimensional model described in [section 3](#) reached thermobarically unstable conditions before the end of August



Click on thumbnail for full-sized image.

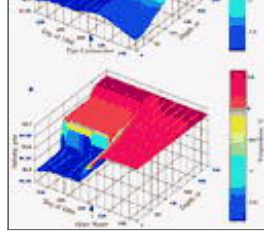
Fig. 9. Thermobaric barrier diagram for station YU043, illustrating an example that is stable despite a relatively high value for  $\theta_{\text{plume}}$  (7.4) because of the substantial thermal barrier between the mixed layer and the  $\Delta\rho_{\text{max}}$  level



Click on thumbnail for full-sized image.

Fig. 10. Results from the LTC numerical model described in the text. (a) Friction velocity at the ice–ocean boundary (solid), and conductive heat flux inferred from the buoy ice temperature gradient (dashed). The driving time series are from [McPhee et al. \(1999\)](#). (b) Modeled ice thickness and ocean-to-ice heat flux. (c) Modeled mixed layer depth, based on the density gradient (solid) and on the difference between salinity and near-surface salinity (dashed). Type I convection into the lower step layer begins on day 231. (d) The mass deficit (dashed) and thermobaric barrier (solid). The circled time (day 227, 15 Aug 94) indicates when modeled conditions would instigate Type II convection





Click on thumbnail for full-sized image.

Fig. 11. (a) Modeled salinity ( $z$  ordinate) and temperature (color intensity according to the scale at the right) for the model run of Fig. 10, which neglects thermobaric effects. The mixed layer becomes dense enough by day 231 to allow Type I convection into the layer below, with rapid mixing. (b) Like (a) except that the model sets eddy heat and salt diffusivity to uniformly high values after the onset of thermobaric instability at time 227.75

<sup>1</sup> It is not clear from their analysis, however, how negative buoyancy flux from cooling needed to maintain Type I convection would counteract the strong positive buoyancy flux from ice melt, as soon as the ice grew enough to trigger convection.

Corresponding author address: Dr. Miles G. McPhee, McPhee Research Company, 450 Clover Springs Road, Naches, WA 98937.

E-mail: [miles@apl.washington.edu](mailto:miles@apl.washington.edu)

top ▲



© 2008 American Meteorological Society [Privacy Policy and Disclaimer](#)  
Headquarters: 45 Beacon Street Boston, MA 02108-3693  
DC Office: 1120 G Street, NW, Suite 800 Washington DC, 20005-3826  
[amsinfo@ametsoc.org](mailto:amsinfo@ametsoc.org) Phone: 617-227-2425 Fax: 617-742-8718  
[Allen Press, Inc.](#) assists in the online publication of AMS journals.